Mechanics of Advanced Composite Structures

Journal homepage: https://macs.semnan.ac.ir/

Semnan University

ISSN: 2423-7043

Research Article

Investigation of Vibration Energy Harvesting in Multilayer Composite Plates with Anisotropic Piezoelectric Patches

Asghar Jamshiddoust, Morteza Karamooz Mahdiabadi, Amin Farrokhabadi *

Department of Mechanical Engineering, Tarbiat Modares University, P.O. Box 14115-177, Tehran, Iran

ARTICLE INFO

Article history:

Received: 2024-04-06

Revised: 2024-08-23

Accepted: 2024-10-10

Keywords:

Piezoelectric patch;

Anisotropic effect;

Output voltage;

Vibration;

Composite plate.

ABSTRACT

This study investigates the impact of anisotropic and isotropic piezoelectric coefficients on vibrational energy harvesting using a piezoelectric patch integrated into plate-like structures. The research on energy harvesting in such configurations has garnered substantial attention in recent decades, with previous studies typically assuming isotropic piezoelectric coefficients ($e_{31} = e_{32}$). The investigation focuses on two common boundary conditions: cantilevered composite plate (CFFF) and all-four-edges clamped (CCCC), employing a combination of analytical techniques and numerical simulations. The study presents comprehensive steady-state formulations for both the electrical and structural responses under harmonic force excitation. By comparing the voltage-frequency relationship between the analytical and numerical models, the accuracy of the analytical electroelastic model is verified. The findings highlight the potential for enhanced performance and increased output voltage in CFFF structures with an approximate rate between 5% to 8 % by minimizing the impact of the e_{32} coefficient, whereas a decrease in output voltage is observed in CCCC structures. The findings emphasize that minimizing the impact of specific piezoelectric coefficients can lead to significant improvements in both performance and output voltage. This contributes to advancements in energy harvesting technology, highlighting the importance of optimizing piezoelectric materials to achieve better efficiency in energy harvesting applications. Additionally, the study shows that reducing the effects of e_{32} in anisotropic piezoelectric harvesters can enhance energy harvesting from the vibration of a multilayer composite cantilevered plate. This research contributes valuable insights into optimizing piezoelectric energy harvesting efficiency in plate-like structures, paving the way for advancements in energy harvesting technology.

1. Introduction

Low-power applications and self-powered systems, which can be supported using the energy available in their environment, especially vibrational energy, have attracted significant attention in recent years. This feature motivated researchers to design energy harvesters such as vibrational energy harvesting with piezoelectric materials due to their efficiency and favorable frequency response. In this regard, various studies have been done to improve the efficiency and bandwidth of piezoelectric energy harvesters [1-7].

In recent years, some researchers have studied anisotropic effects in the performance of sensors and piezoelectric energy harvesters. Also, efforts have been made to make different types of materials with anisotropic

* **Corresponding author.**
E-mail address: *Amin-farrokh@modares.ac.ir*

Cite this article as:
Jamshiddoust, A., Karamooz Mahdiabadi, M. and Farrokhabadi, A., 2025. Investigation of vibration energy harvesting in multilayer composite plates with anisotropic piezoelectric patches. *Mechanics of Advanced Composite Structures*, 12(1), pp. 223-234.
https://doi.org/10.22075/MACS.2024.33713.1633

piezoelectricity [8-11]. It is shown that directional piezoelectric can enhance the control performance of the piezoelectric actuators [12]. Roscow et al. [13] studied the piezoelectric anisotropy and energy-harvesting characteristics of novel sandwich layer BaTiO3 structures.

Some amount of piezoelectric anisotropy can be achieved by directionally attaching the piezo crystal to the substrate [14]. Also, the e_{32}-based effect in a discrete monolithic piezoelectric crystal can be reduced by partially bonding along its width, which will result in mainly the longitudinal strain and will be influenced by the piezoelectric constant e_{31}. It is worth mentioning that e_{31} and e_{32} represent the piezoelectric transversal effect, i.e., a deformation is generated perpendicular to the applied electric field. By developing piezoelectric composite plies, a more realistic way of piezoelectric anisotropy can be achieved, which is demonstrated by Hagood et al. [15-16]. The piezoelectric anisotropy can be introduced by properly orienting the active ply in the smart laminated composites since the piezoelectric composite ply has the property $e_{31} \neq e_{32}$.

In the previous research in developing analytical models for energy harvesting from the vibrations of metal or composite plates, isotropic piezoelectric patch assumptions have been used [17-19]. In recent years researchers have delved into novel strategies to enhance sensor and energy harvester performance by leveraging directional piezoelectricity and anisotropic materials (20-22). These studies illuminate the potential for enhancing sensing performance and energy-harvesting characteristics through tailored material design and orientation, paving the way for innovative applications in the field. Their findings demonstrated significant improvements in output voltage and energy harvesting capabilities.

Since piezoelectric patch harvesters attached to thin plates can be easily integrated, they are more convenient than other traditional energy harvesting using piezoelectric cantilevers for use in marine, aerospace, and automotive applications. These systems are often composed of thin plate-like structures with various boundary conditions, and energy harvesting can be done without mass loading and volumetric occupancy of base-excited cantilever attachments.

This advantage makes them well suited for smart structures in aerospace, marine, and automotive applications such as structural health monitoring, energy harvesting, and vibration control to exploit structural vibration modes of the host system directly. Integrating piezo-patch energy harvesters into plate-like structures eliminates the mass loading and volumetric occupancy of cantilever attachments [23- 24].

It should be noted that the anisotropy is not only a relationship between $e_{32}$and e_{31}, and it is also more of a material science problem which helps highlight other effects that may show up due to changes in e_{32}. Analytical models that can consider anisotropic effects in piezoelectric materials provide much more efficient methods for designing and developing piezoelectric structures according to the intended application. The plate equations of a structure are written in order to study the anisotropic effects of piezoelectric materials analytically. Compared to a large number of studies focused on piezoelectric energy harvester beams [25-28], very limited research has been done on plate-like piezoelectric energy harvesters.

This work presents an analytical electroelastic model of a thin multilayer plate with a piezoelectric patch using the classical laminate plate theory and modal analysis procedure. Closed-form steady-state expressions for the electrical and structural responses are presented for harmonic force excitation. Voltage vs. frequency from the analytical model is compared with the numerical model to show the accuracy of the analytical electroelastic model. To study the piezoelectric anisotropy effects, both the e_{31} and e_{32} modes are considered in the equations of the output voltage of the piezoelectric patch. The effect of different amounts of e_{32} is investigated to increase the output voltage of the piezoelectric energy harvesters. Furthermore, in order to verify the results obtained from the analytical solution, the finite element analysis of the piezoelectric energy harvester is performed using ANSYS.

The novelty of this study lies in the investigation of the impact of anisotropic and isotropic piezoelectric coefficients on vibrational energy harvesting using piezoelectric patches integrated into plate-like structures. While previous research predominantly assumed isotropic piezoelectric coefficients, this study delves into the effects of anisotropy, particularly focusing on the e_{32} coefficient. By exploring two common boundary conditions, namely cantilevered composite plate (CFFF) and all-four-edges clamped (CCCC), this study provides a comprehensive analysis of the electrical and structural responses under harmonic force excitation. The incorporation of analytical techniques and numerical simulations allows for a detailed comparison of the voltage-frequency relationship between the analytical and numerical models.

2. Electroelastic Modeling in Physical Coordinates

Most of the models for the analysis of piezoelectric energy harvesters have been derived for the beams; however, it is necessary to write plate equations for energy harvesters to investigate specific applications such as activation of the d_{32} mode of the piezoelectric. For this purpose, the piezoelectric patch mounted on a multilayer composite plate with cantilever boundary conditions is investigated, as shown in Fig. 1.

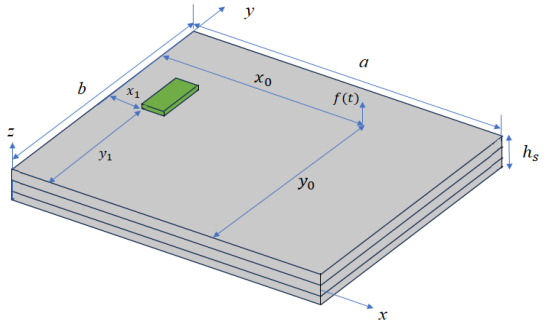

Fig. 1. Installation conditions of piezoelectric patch on multilayer composite plate with cantilever boundary conditions

The governing partial differential equation of forced vibration of a thin multilayer composite plate with a small piezoelectric patch can be written as [17].

$$\frac{\partial^2 (M_1{}^s + M_1{}^p)}{\partial x^2} + 2\frac{\partial^2 (M_6{}^s + M_6{}^p)}{\partial x \partial y} + \frac{\partial^2 (M_2{}^s + M_2{}^p)}{\partial y^2} - c\frac{\partial w(x,y,t)}{\partial t} - m\frac{\partial^2 w(x,y,t)}{\partial t^2} + f(t)\delta(x-x_0)\delta(y-y_0) = 0 \quad (1)$$

where superscripts "s" and "p" represent the substructure and piezoelectric patch, respectively. $w(x,y,t)$ is the transverse deflection of the plate at position (x,y) and time (t). The internal bending moments are M_1, M_2 along x and y axis, and M_6 is the shear bending in the x–y plane. The mass per unit area of the plate is m and c is the viscous damping coefficient. The location of the transverse point load $f(t)$ along the x and y directions is defined by Dirac delta functions $\delta(x)$ and $\delta(y)$. This force is acting at (x_0, y_0).

The internal bending moments of the host structure can be expressed in terms of curvatures based on classical laminate plate theory as follows [19]:

$$\begin{aligned} M_1^s &= D_{11}\kappa_x + D_{12}\kappa_y \\ M_2^s &= D_{12}\kappa_x + D_{22}\kappa_y \\ M_6^s &= 2D_{66}\kappa_{xy} \end{aligned} \quad (2)$$

By considering the formula of mid-plane curvatures of the plate, the bending moments in terms of transverse deflection can be written as [19]

$$\begin{aligned} M_1^s &= -D_{11}\frac{\partial^2 w(x,y,t)}{\partial x^2} - D_{12}\frac{\partial^2 w(x,y,t)}{\partial y^2} \\ M_2^s &= -D_{12}\frac{\partial^2 w(x,y,t)}{\partial x^2} - D_{22}\frac{\partial^2 w(x,y,t)}{\partial y^2} \\ M_6^s &= -2D_{66}\frac{\partial^2 w(x,y,t)}{\partial x \partial y} \end{aligned} \quad (3)$$

where D_{ij} are the bending stiffness terms and calculated for each layer of the host plate as [19]

$$D_{ij} = \frac{1}{3}\sum_{k=1}^{n}\left(\overline{Q}_{ij}\right)_k (h_k^3 - h_{k-1}^3) \quad (4)$$

and the $\overline{Q}_{ij}$ parameters which are the components of the transformed ply stiffness matrix of the orthotropic ply are determined as [19]

$$\bar{Q}_{11} = Q_{11}\cos^4\theta + 2(Q_{12} + 2Q_{66})\sin^2\theta \times \cos^2\theta + Q_{22}\sin^4\theta \quad (5)$$

$$\bar{Q}_{12} = (Q_{11} + Q_{12} - 4Q_{66})\sin^2\theta\cos^2\theta + Q_{22}(\cos^4\theta + \sin^4\theta) \quad (6)$$

$$\bar{Q}_{22} = Q_{11}\sin^4\theta + 2(Q_{12} + 2Q_{66})\sin^2\theta \times \cos^2\theta + Q_{22}\cos^4\theta \quad (7)$$

$$\bar{Q}_{66} = (Q_{11} + Q_{22} - 2Q_{12} - 2Q_{66})\sin^2\theta \times \cos^2\theta + Q_{66}(\cos^4\theta + \sin^4\theta) \quad (8)$$

in which θ is the off-axis orthotropic ply angle and,

$$Q_{11} = \frac{E_1}{1 - \nu_{12}\nu_{21}}$$

$$Q_{12} = \frac{\nu_{12} \times E_2}{1 - \nu_{12}\nu_{21}}$$

$$Q_{22} = \frac{E_2}{1 - \nu_{12}\nu_{21}}$$

$$Q_{66} = G_{12}$$

The internal moments of the piezoceramic patch are [19]:

$$M_1^P = [H(x-x_1) - H(x-x_2)][H(y-y_1) - H(y-y_2)] \int T_1^P \, z \, dz \tag{9}$$

$$M_2^P = [H(x - x_1) - H(x - x_2)] \times [H(y - y_1) - H(y - y_2)] \int T_2^P \, z \, dz \tag{10}$$

$$M_6^P = [H(x - x_1) - H(x - x_2)] \times [H(y - y_1) - H(y - y_2)] \int T_6^P z dz \tag{11}$$

where $H(x)$ and $H(y)$ are the Heaviside functions, and the integrals are over the thickness of piezoceramic patch.

The linear piezoelectric constitutive equations of a thin piezoceramic patch attached to the host plate can be written as [29]

$$\begin{bmatrix} T_1^p \\ T_2^p \\ T_6^p \\ D_3 \end{bmatrix} = \begin{bmatrix} \bar{C}_{11}^{E} & \bar{C}_{12}^{E} & 0 & -\bar{e}_{31} \\ \bar{C}_{12}^{E} & \bar{C}_{22}^{E} & 0 & -\bar{e}_{32} \\ 0 & 0 & \bar{C}_{66}^{E} & 0 \\ -\bar{e}_{31} & -\bar{e}_{32} & 0 & \bar{\varepsilon}_{33}^{S} \end{bmatrix} \begin{bmatrix} S_1^p \\ S_2^p \\ S_6^p \\ E_3 \end{bmatrix} \tag{12}$$

where T_1^P and T_2^P represent the normal stress components along x and y axes respectively, T_6^P is the shear stress in the $x-y$ plane, D_3 is the electric displacement in z-direction (poling direction of piezoceramic patch), S_1^P and S_2^P are the normal strain components along the x and y axes, S_6^P is the shear strain component in the $x-y$ plane, and E_3 is the electric field in the thickness direction. The effective piezoelectric stress constants are $\bar{e}_{31}$ and $\bar{e}_{32}$, elastic stiffness components are $\bar{C}_{11}^E$, $\bar{C}_{12}^E$ and $\bar{C}_{66}^E$ and the $\bar{\varepsilon}_{33}^S$ is the permittivity component. The superscript "P" represents the piezoceramic patch, while "E" and "S" denote the respective parameters obtained at the constant electric field and constant strain, respectively.

The reduced elastic, piezoelectric, and permittivity constants, which are reduced to two-dimensional (2D) form three-dimensional (3D) electroelasticity components, can be written as [30]

$$\begin{aligned} \bar{C}_{11}^E &= C_{11}^E - \frac{(C_{13}^E)^2}{C_{33}^E} \ , \\ \bar{C}_{12}^E &= C_{12}^E - \frac{C_{13}^E C_{23}^E}{C_{33}^E} \ , \\ \bar{C}_{22}^E &= C_{22}^E - \frac{(C_{23}^E)^2}{C_{33}^E} \ , \quad \bar{C}_{66}^E = C_{66} \ , \\ \bar{\varepsilon}_{33}^S &= \varepsilon_{33}^S + \frac{e_{33}^2}{C_{33}^E} \ , \\ \bar{e}_{31} &= e_{31} - \frac{C_{13}^E e_{33}}{C_{33}^E} \ , \quad \bar{e}_{32} = e_{32} - \frac{C_{23}^E e_{33}}{C_{33}^E} \end{aligned} \tag{13}$$

By substituting the internal moments of the host plate and the piezoceramic patch into equation (1), the governing partial differential equation of the multilayer plate with piezoelectric coupling is derived as

$$\begin{aligned} & D_{11} \frac{\partial^4 w(x,y,t)}{\partial x^4} + 2(D_{12} + 2D_{66}) \frac{\partial^4 w(x,y,t)}{\partial x^2 \partial y^2} \\ & + D_{22} \frac{\partial^4 w(x,y,t)}{\partial y^4} + C \frac{\partial w(x,y,t)}{\partial t} \\ & + \rho_s h_s \frac{\partial^2 w(x,y,t)}{\partial t^2} - v(t) \\ & \times \left\{ \chi_1 \left[\frac{d\delta(x-x_1)}{dx} - \frac{d\delta(x-x_2)}{dx} \right] [H(y-y_1) - H(y-y_2)] \right. \\ & \left. + \chi_2 [H(x-x_1) - H(x-x_2)] \left[\frac{d\delta(y-y_1)}{dy} - \frac{d\delta(y-y_2)}{dy} \right] \right\} \\ & = f(t) \, \delta(x - x_0) \, \delta(y - y_0) \end{aligned} \tag{14}$$

where the electromechanical term χ is defined as the multiplication of effective piezoelectric constant $\bar{e}_{31}$ and reference distance h_{pc}.

$$\chi_1 = \bar{e}_{31} h_{pc}$$

$$\chi_2 = \bar{e}_{32} h_{pc}$$

The reference distance h_{pc} is the distance from the neural surface of the host plate to the center plane of the piezoelectric patch. Another equation to solve the problem is the electrical coupling equation which can be derived based on the piezoelectric constitutive equation for the thin plate as follows [17]

$$\begin{aligned} & Cp \frac{dv(t)}{dt} + \frac{v(t)}{R} \\ & + \left\{ \int_{y_1}^{y_2} \int_{x_1}^{x_2} \left[\chi_1 \frac{\partial^3 w(x,y,t)}{\partial x^2 \partial t} \right. \right. \\ & \left. \left. + \chi_2 \frac{\partial^3 w(x,y,t)}{\partial y^2 \partial t} \right] dxdy \right\} = 0 \end{aligned} \tag{15}$$

where R is the electric resistance and C_p is the electrical capacitance of piezoelectric patch. These electroelastic equations represent the distributed parameter model of the composite plate with a piezoceramic patch in physical coordinates and can be solved using modal analysis.

2.1. Governing Equations in Modal Coordinates

By using the modal analysis, the deflection of the multilayer host plate is given as

$$w(x,y,t) = \sum_{m=1}^{p}\sum_{n=1}^{q} \varphi_{mn}(x,y)\,\eta_{mn}(t) = \sum_{m=1}^{p}\sum_{n=1}^{q} A_{mn}\mathrm{X_m}(x)Y_n(y)\eta_{mn}(t) \quad (16)$$

where the eigenfunctions for the cantilevered plate (CFFF) are calculated as [31]

$$X_m(x) = \cosh\left(\lambda_m\frac{x}{a}\right) - \cos\left(\lambda_m\frac{x}{a}\right) - \alpha_m\left[\sinh\left(\lambda_m\frac{x}{a}\right) - \sin\left(\lambda_m\frac{x}{a}\right)\right]. \quad (17)$$

Moreover, the eigenfunctions for the plate with free-free boundary conditions are

$$Y_1(y) = 1, \quad (18a)$$

$$Y_2(y) = \sqrt{3}\left(1 - \frac{2y}{b}\right), \quad (18b)$$

$$Y_n(y) = \cosh\left(\mu_n\frac{y}{b}\right) + \cos\left(\mu_n\frac{y}{b}\right) - \beta_n\left[\sinh\left(\mu_n\frac{y}{b}\right) + \sin\left(\mu_n\frac{y}{b}\right)\right] \ (n=3, 4, 5,\ldots). \quad (18c)$$

The first two equations in (18) represent the rigid-body translation and rotation, respectively. The parameter a is the length, and b is the width of the plate.

Similarly, for the all-four-edges clamped plate (CCCC), both of the eigenfunction components can be presented as in (17). The modal amplitude constant (A_{mn}) can be calculated by normalizing the eigenfunctions by the orthogonality conditions.

$$\int_0^b\int_0^a \rho_s h_s\,\varphi_{mn}(x,y)\varphi_{rs}(x,y)\,dx\,dy = \delta_{mr}\,\delta_{ns}$$

$$\int_0^b\int_0^a \left(D_{11}\frac{d^2\varphi_{mn}(x,y)}{d_x^2}\frac{d^2\varphi_{rs}(x,y)}{d_x^2} + 2\,(D_{12} + 2D_{66})\frac{d^2\varphi_{mn}(x,y)}{d_x^2}\frac{d^2\varphi_{rs}(x,y)}{d_y^2} + D_{22}\frac{d^2\varphi_{mn}(x,y)}{d_y^2}\frac{d^2\varphi_{rs}(x,y)}{d_y^2}\right)dx\,dy = \omega_{mn}^2\,\delta_{mr}\,\delta_{ns} \quad (19)$$

the δ_{mr} and δ_{ns} are Kronecker delta functions, which are equal to unity for $m = r$ and $n = s$, respectively. Similarly, they are equal to zero for $m \neq r$ and $n \neq s$. The undamped natural frequency of the $mn-th$ vibration mode of the multilayer plate in short-circuit conditions can be obtained as [19]

$$\omega_{mn} = \sqrt{\frac{D_{11}(\lambda_m)^4 + 2(D_{12} + 2D_{66})(\lambda_m)^2(\mu_n)^2 + D_{22}(\mu_n)^4}{\rho_s h_s}} \quad (20)$$

The electromechanically coupled ordinary differential equation of the multilayer plate can be obtained in modal space by following the modal analysis procedure [32] and multiplying the partial differential equations in physical coordinates by eigenfunction $\varphi_{mn}(x,y)$ and integrating over the surface area of the plate.

$$\frac{d^2\eta_{mn}}{dt^2} + 2\zeta_{mn}\omega_{mn}\frac{d\eta_{mn}}{dt} + \omega_{mn}^2\eta_{mn}(t) - \chi_{mn}v(t) = f_{mn}(t) \quad (21)$$

where η_{mn} is the modal time response and ζ_{mn} is the modal damping ratio and can be obtained by using the damping identification techniques. The modal forcing and electromechanical coupling terms are defined as

$$f_{mn} = \int_0^b\int_0^a f(t)\delta(x - x_0)\delta(y - y_0) \times \varphi_{mn}(x,y)dx\,dy = f(t)\varphi_{mn}(x_0,y_0)$$

$$\chi_{mn} = \left[\chi_1\int_{y_1}^{y_2}\frac{\partial\varphi_{mn}(x,y)}{\partial x}\Big|_{x_1}^{x_2}dy + \chi_2\int_{x_1}^{x_2}\frac{\partial\varphi_{mn}(x,y)}{\partial y}\Big|_{y_1}^{y_2}dx\right] \quad (22)$$

which shows that the slope of mode shapes φ_{mn} along the edges of the piezoceramic patch together with the covered region specifies the electromechanical coupling term.

By substituting the modal expansion into the electrical coupling equation, the governing equation of the electrical circuit in modal coordinates can be written as

$$C_p\frac{dv(t)}{dt} + \frac{v(t)}{R} + \sum_{n=1}^{\infty}\sum_{m=1}^{\infty}\chi_{mn}\frac{d\eta_{mn}(t)}{dt} = 0 \quad (23)$$

As a result, the two governing equations of a thin multilayer composite plate with a piezoelectric patch are obtained in the modal coordinates.

3. Steady-State Solution

By assuming the harmonic force excitation as $f(t) = F_0 e^{j\omega t}$ (the force amplitude is F_0 and ω is the excitation frequency) and linear oscillations, the steady-state response of modal and voltage can be obtained as [17]

$$\eta_{mn}(t) = H_{mn}e^{jwt}, \quad v(t) = V_0 e^{jwt} \quad (24)$$

By substituting these modal and voltage expressions into the electromechanical coupled governing equations in the modal space

(equations (21) and (23)), the amplitudes H_{mn} and V_0 are determined as

$$H_{mn} = \frac{F_0\varphi_{mn}(x_0,y_0) + \chi_{mn}V_0}{\omega_{mn}^2 - \omega^2 + j2\zeta_{mn}\omega_{mn}\omega}$$
$$V_0 = \frac{-j\omega \sum_{m=1}^{\infty}\sum_{n=1}^{\infty}\frac{F_0\varphi_{mn}(x_0,y_0)\chi_{mn}}{\omega_{mn}^2-\omega^2+2\,j\zeta_{mn}\omega_{mn}\omega}}{\frac{1}{R}+j\omega C_p+j\omega\sum_{m=1}^{\infty}\sum_{n=1}^{\infty}\frac{j\omega\chi_{mn}^2}{\omega_{mn}^2-\omega^2+2\,j\zeta_{mn}\omega_{mn}\omega}} \quad (25)$$

Using the closed-form steady-state expression of the voltage across the resistive load, the instantaneous power output $P(t)$ generated by the piezoceramic patch can be calculated as

$$P(t) = \frac{v^2(t)}{R}$$

By substituting the modal and voltage response into the host plate deflection equation, the transverse deflection of the multilayer plate is calculated as

$$w(x,y,t) = \sum_{m=1}^{\infty}\sum_{n=1}^{\infty}\left(\varphi_{mn}(x_0,y_0) - \frac{j\omega\sum_{n=1}^{\infty}\sum_{m=1}^{\infty}\chi_{mn}\frac{\varphi_{mn}(x_0,y_0)}{\omega_{mn}^2-\omega^2+2\,j\zeta_{mn}\omega_{mn}\omega}}{\frac{1}{R}+j\omega C_p+j\omega\sum_{m=1}^{\infty}\sum_{n=1}^{\infty}\frac{j\omega\chi_{mn}^2}{\omega_{mn}^2-\omega^2+2\,j\zeta_{mn}\omega_{mn}\omega}}\right)\times \frac{F_0\varphi_{mn}(x,y)e^{jwt}}{\omega_{mn}^2-\omega^2+2\,j\zeta_{mn}\omega_{mn}\omega} \quad (26)$$

4. Finite Element Model for the Voltage Calculation of Energy Harvester

In order to verify the results obtained from the analytical solution we use the finite element model of the piezoelectric energy harvester, which is performed in ANSYS. Three different types of elements, including 120 solid226 as the piezoelectric elements, 5800 solid186 as the structural elements determined by a convergence test, are used in the model, which can be seen in Fig. 2. The resistance between the top and bottom electrodes is simulated by one CIRCU94 element which represents the voltage coupling between the top and bottom surfaces of the piezoelectric patch with two nodes and can interface with the piezoelectric element. The amplitude, mode shapes and output voltage are obtained from the finite element analysis. The composite substructure plate investigated in this study is made of three layers of fiber woven. The properties of the composite plate and piezoelectric patch are given in Table 1. The properties of the glass/epoxy lamina have already been obtained by experimental characterization tests [33].

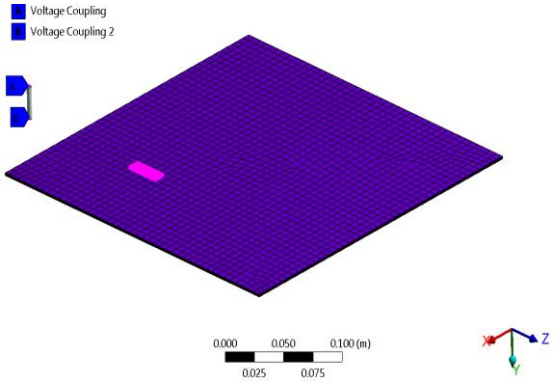

Fig. 2. Finite element model of the composite substrate and piezoelectric patch with the voltage coupling between the piezoelectric and circuit element

Table 1. PZT patch and composite substrate properties

Parameters			Symbol	Value	Unit
Material		Piezoelectric electromechanical coupling	d_{31}	-97×10^{-12}	C/N
	PZT-5H	Density	ρ	7750	Kg/m^3
		Young Modulus in the longitude direction	$E_{11,p}$	120.35	GPa
		Young Modulus in the lateral direction	$E_{22,p}$	75.18	GPa
	Woven fabric	Poisson's ratio	$\nu_{12}=\nu_{21}$	0.31	---
		Young Modulus (x_1)	E_1	22.688	GPa
		Young Modulus (x_2)	E_2	22.688	GPa
		Young Modulus (x_3)	E_3	2.700	GPa
		Young Modulus (x_2x_3)	G_{23}	1.600	GPa
		Young Modulus (x_3x_1)	G_{31}	5.494	GPa
		Young Modulus (x_1x_2)	G_{12}	5.494	GPa
		Poisson's ratio (x_2x_3)	ν_{23}	0.1	---
		Poisson's ratio (x_3x_1)	ν_{31}	0.1	---
		Poisson's ratio (x_1x_2)	ν_{12}	0.144	---
		Density	ρ	1476	Kg/m^3

	Resistance Load	R	8000	Ohm
Physical properties	Piezoelectric layer thickness	h_p	1	mm
	Substrate layer thickness	h_s	0.7	mm
	Permittivity	ε_0	8.854×10^{-12}	---
	Plate length	a	300	mm
	Plate width	b	300	mm
	Damping ratio	d_{11}	0.01	---
	Piezoelectric patch length	L_p	30	mm
	Piezoelectric patch width	W_p	10	mm
	Excitation force location (CFFF plate)	(x_0, y_0)	(a, b/2)	mm
	Excitation force location (CCCC plate)	(x_0, y_0)	(a/2, b/2)	mm
	Piezoelectric patch location on the plate	(x_1, y_1)	(a/4, b/4)	mm
	Amplitude of excitation force	F_0	0.1	N

5. Results and Discussion

Analytical solutions, such as the one presented in Equation (26), provide valuable insights into the behavior of piezoelectric energy harvesters under different operating conditions. However, to validate these analytical results and obtain a more comprehensive understanding of the system's performance, numerical methods like finite element analysis become essential. The finite element model described in Section 4 by integrating multiphysics simulations that consider electromechanical coupling effects can enhance the predictive capabilities of finite element models. This analysis offers a detailed representation of the energy harvester's behavior and allows for a thorough investigation of its voltage generation capabilities.

In this section, the analytical solution for calculating the output voltage and the mode shapes of the multilayer composite plate is investigated by comparison with the finite element analysis. The normalized mode shapes for the two modes of the CFFF plate from the analytical method as well as the finite element analysis, are shown in Fig. 3 and Fig. 4, respectively.

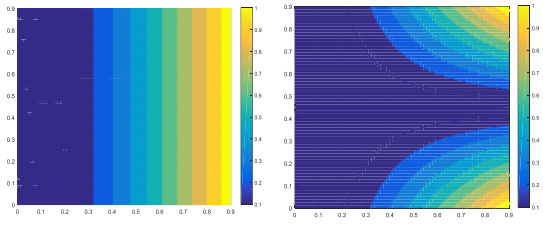

$(a)\omega_{11}$ $(b)\omega_{12}$

Fig. 3. Normalized mode shapes for the (a) first, and (b) second modes of the CFFF plate from the analytical solution

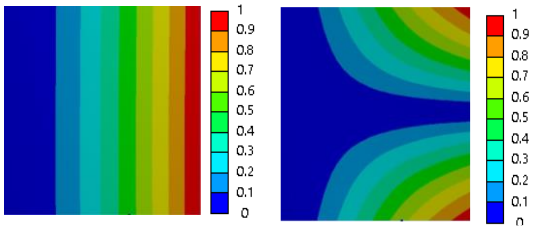

$(a)\omega_{11}$ $(b)\omega_{12}$

Fig. 4. Normalized mode shapes for the (a) first, and (b) second modes of the CFFF plate from FEM

The normalized mode shapes for the two modes of the all-four-edges clamped (CCCC) plate from the analytical method as well as the finite element analysis are shown in Fig. 5 and Fig. 6, respectively.

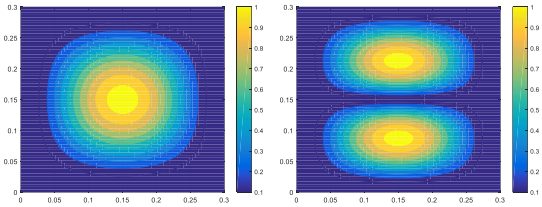

$(a)\omega_{11}$ $(b)\omega_{12}$

Fig. 5. Normalized mode shapes for the (a) first, and (b) second modes of the CCCC plate from the analytical solution

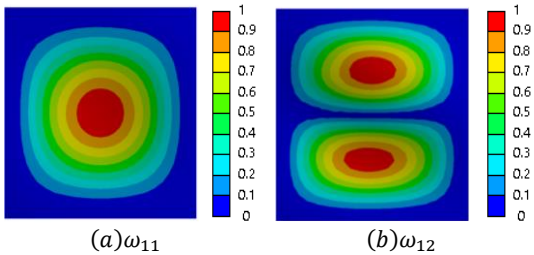

$(a)\omega_{11}$ $(b)\omega_{12}$

Fig. 6. Normalized mode shapes for the (a) first, and (b) second modes of the CCCC plate from FEM

By comparing Fig. 3 and Fig. 4, as well as Fig. 5 and Fig. 6, it can be seen that the mode shapes obtained by the analytical model match well with those of the finite element results. The output voltage vs. excitation frequency for the first mode of the isotropic piezoelectric patch ($e_{32} = e_{31}$) integrated on the cantilevered composite plate (CFFF) using the analytical solution and finite element analysis are shown in Fig. 7.

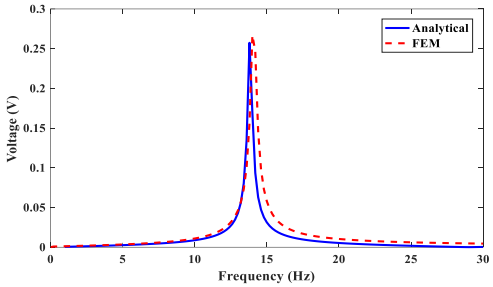

Fig. 7. The output voltage of the isotropic piezoelectric energy harvester integrated on the cantilevered plate (CFFF) vs. excitation frequency from Analytical solution and FEA

As can be seen, there is a good agreement between the voltage spectrum by the analytical model and finite element results, with an approximately 1.8 % difference in the calculated resonance frequency. The analytical and FEA models predict the 1st resonance frequency as 13.83 Hz and 14.08 Hz, respectively.

The slight difference is mainly due to neglecting the piezoceramic patch's inertial and stiffness in the analytical model, while they are considered in the finite element analysis. Note that the volume of the piezoceramic patch is assumed to be significantly smaller than the host plate, and the inertia and stiffness of the piezoelectric patch are neglected because of their small effect on natural frequency and neutral axis.

The output electrical voltage of the piezoelectric patch integrated on the cantilevered composite plate (CFFF) for different values of e_{32} from finite element analysis is shown in Fig. 8-a. In addition, the output voltage versus excitation frequency for different values of e_{32} from the analytical method is shown in Fig. 8-b. The predicted output voltage from the analytical method is in good agreement with the finite element analysis results for different values of e_{32}.

It can be observed that decreasing e_{32} will cause an increase in the output voltage of the piezoelectric patch. In both cases, including the analytical method and finite element analysis, it is shown that decreasing the e_{32} to $e_{31}/2$ and then from $e_{31}/2$ to zero will increase the output voltage with an approximate rate between 5 to 8 %. With a 2 % amount of difference, both analyses show that reducing the effect of e_{32} will increase the output voltage of the energy harvester.

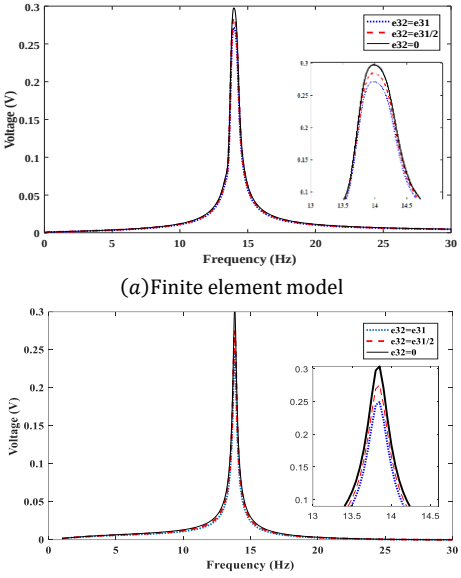

(a)Finite element model

(b)Analytical model

Fig. 8. Effect of different values of e_{32} on the output voltage of the piezoelectric patch integrated on the CFFF composite plate from (a) finite element analysis, and (b) analytical model

The effect of different values of e_{32} on the impedance amplitude and phase angle of the piezoelectric energy harvester, which are derived from finite element analysis, can be seen in Fig. 9. As can be seen, a phase change occurs near the resonance frequency, where we see the maximum value of the oscillation amplitude. It is shown that the impedance amplitude will increase by decreasing e_{32} while there is no significant change in the phase angle value.

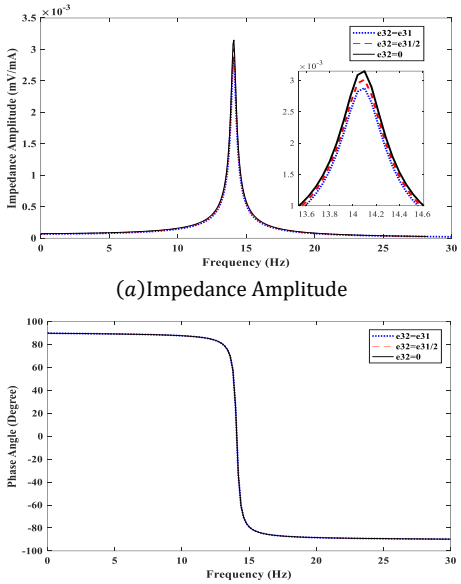

(a)Impedance Amplitude

(b)Phase Angle

Fig. 9. Effect of different values of e_{32} on the (a)Impedance Amplitude, and (b) Phase Angle of the piezoelectric patch attached to the CFFF plate from the FEA

The summary of the obtained results and the corresponding peak voltage of each case are

shown in Table 2. By comparison of the peak values of the voltage of the piezoelectric patch at different e_{32} values obtained from the finite element analysis (FEA) and the analytical model, it can be observed that in Case 1, where e_{32} is equal to e_{31}, the FEA yields a maximum voltage of 0.2668, while the Analytical model shows a slightly lower peak voltage of 0.2514. Moving to Case 2 with e_{32} equal to $e_{31}/2$, the FEA results in a higher maximum voltage of 0.2795 compared to the Analytical model's peak voltage of 0.2602. In Case 3, setting e_{32} to 0, the FEA demonstrates the highest maximum voltage of 0.2923, and the Analytical method follows with a peak voltage of 0.2720. The comparison between the FEA and analytical results shows variations in the obtained maximum voltages for each case. The FEA tends to provide slightly higher peak voltage values compared to the analytical method. These differences can be attributed to the inherent approximations and assumptions made in the analytical model, leading to minor discrepancies in the predicted peak voltages as opposed to the more detailed simulations in the FEA.

Table 2. The maximum output voltage of the piezoelectric patch at different e_{32} values

Case	e_{32} value	Max. voltage (V)-FEA	Max. voltage (V)-Analytical
1	$e_{32} = e_{31}$	0.2668	0.2514
2	$e_{32} = \frac{e_{31}}{2}$	0.2795	0.2602
3	$e_{32} = 0$	0.2923	0.2720

The output electrical voltage of the piezoelectric patch integrated on all four edges clamped composite plate (CCCC) for different values of e_{32} from finite element analysis is shown in Fig. 10-a. In addition, the output voltage versus excitation frequency for different values of e_{32} from the analytical method is shown in Fig. 10-b. The predicted output voltage from the analytical method has a difference of about 2-5 % with the finite element analysis results for different values of e_{32}.

It can be observed that decreasing e_{32} will cause a decrease in the output voltage of the piezoelectric patch integrated into the CCCC composite plate. In both cases, including the analytical method and finite element analysis, it is shown that decreasing the e_{32} to $e_{31}/2$ and then to zero will decrease the output voltage. With a 2-5 % amount of difference, both analyses show that reducing the effect of e_{32} will decrease the output voltage of the piezoelectric energy harvester integrated into the CCCC composite plate.

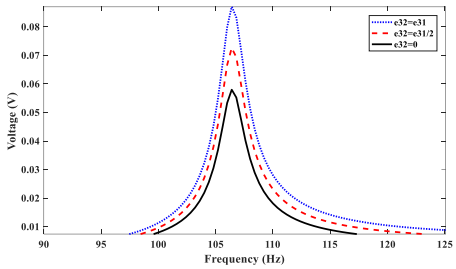

(a)Finite element model

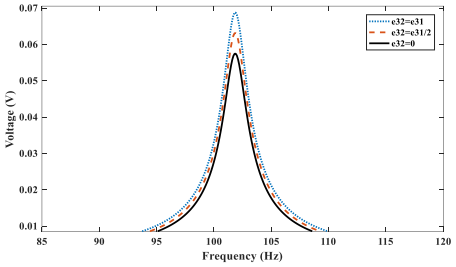

(b)Analytical model

Fig. 10. Effect of different values of e_{32} on the output voltage of the piezoelectric patch integrated on the CCCC composite plate from (a) finite element analysis, and (b) analytical model

The effect of different values of e_{32} on the impedance amplitude and phase angle of the piezoelectric energy harvester, which are derived from finite element analysis, can be seen in Fig. 11. It is shown that the impedance amplitude will decrease by decreasing the e_{32} value while there is no significant change in the phase angle value.

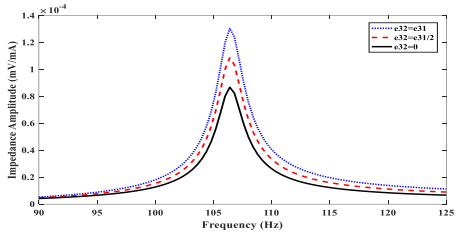

(a)Impedance Amplitude

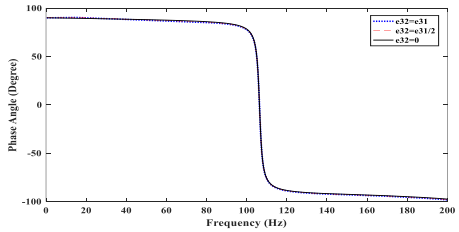

(b)Phase Angle

Fig. 11. Effect of different values of e_{32} on the (a)Impedance Amplitude, and (b) Phase Angle of the piezoelectric patch attached to the CCCC plate from the FEA

It is shown in previous studies [12] that by removing or reducing e_{32}-based piezoelectric effect, better performance control of piezoelectric devices can be achieved. By presenting the obtained results in this study, it can be seen that if e_{32}-based effect is reduced or minimized, in addition to better performance

control achievement of piezoelectric patch integrated on the cantilevered composite plate, the output voltage of piezoelectric-based energy harvesters increases. The results demonstrate that removing or reducing e_{32}-based effect of the piezoelectric patch attached to the all-four-edges clamped (CCCC) plate, the output voltage decreases, indicating that there is no need to reduce the e_{32}-based piezoelectric effect to improve performance in these plates.

Based on the presented results, we conclude that the e_{32} mode causes the dissipation of energy from the piezoelectric patch attached to a cantilevered composite plate, and by removing or reducing the e_{32}-based effect, the output voltage increases. The obtained results show that e_{32} component of piezoelectric acts as a factor of structural damping and dissipates the harvested energy from the vibration of the cantilevered plate. Besides, eliminating the e_{32} mode effect in the cantilevered plate, it is possible to use this mode for increasing the output voltage by implementing the auxetic structures with negative Poisson's ratio as the substrate in the composite plate, which is an ongoing research topic of the authors.

This study presents comprehensive steady-state formulations for both the electrical and structural responses under harmonic force excitation, utilizing a combination of analytical techniques and numerical simulations. By comparing the voltage-frequency relationship between the analytical and numerical models, the accuracy of the analytical electroelastic model is verified. The results demonstrate a good agreement between the analytical model and finite element analysis, with a slight difference attributed to neglecting certain factors in the analytical model. Overall, this study highlights the significance of considering anisotropic effects in piezoelectric materials for optimizing energy harvesting efficiency in plate-like structures. The results suggest that minimizing the e32 coefficient can lead to improved performance and increased output voltage in certain configurations, providing valuable insights for the design and development of piezoelectric energy harvesters.

6. Conclusions

Energy harvesting has gained significant attention in recent years due to its ability to convert ambient energy sources into usable electrical power. Piezoelectric energy harvesters, in particular, have shown promising results in capturing mechanical vibrations and converting them into electrical energy. The efficiency and performance of these systems depend on various factors, including the design of the piezoelectric elements and the structural components used in the energy harvesting device. The impact of anisotropic and isotropic piezoelectric coefficients on vibrational energy harvesting, the analytical and numerical modeling of piezoelectric energy harvesters integrated on plate-like structures, and the potential for enhanced performance and increased output voltage in certain plate configurations have been investigated in this study.

Thin plate structures with various boundary conditions are used in different industries, such as aerospace and automotive applications. Energy harvesting from vibrations of plate-like structures can be very useful in these applications. However, very limited research has been carried out on energy harvesting from the vibration of thin plates. In the previous studies of energy harvesting from the vibrations of plates, isotropic piezoelectric assumptions have been used. We present an analytical model that can consider anisotropic effects in piezoelectric materials and provide an efficient procedure for the development of piezoelectric structures. The e_{32}-based piezoelectric effect can be reduced or modified to increase some percentage in the performance of structures made of piezoelectric materials. It has already been shown that better control of piezoelectric actuators can be obtained by reducing the e_{32} parameter as much as possible.

This study shows that reducing the effects of e_{32} in anisotropic piezoelectric harvesters ($e_{31} \neq e_{32}$), can increase energy harvesting from the vibration of a multilayer composite cantilevered plate. While this method is presented for anisotropic piezoelectric patches on a cantilever plate and an all-four-edges clamped (CCCC) plate, it can also be applied to other boundary conditions of the host plate by considering the relevant modal parameters (natural frequencies, eigenfunctions, and damping coefficients). The results demonstrate that by taking the value of e_{32} as zero in the cantilever plate, the ideal anisotropic piezoelectric can be achieved, which represents a pure uniaxial case. The results obtained from this study can help piezoelectric manufacturers design products with higher efficiency and piezoelectric patches for specific applications. Future studies should focus on further optimizing the design parameters, materials, and operating conditions to maximize the efficiency and practicality of energy harvesting technologies. The proposed model in this paper is demonstrated for the sake of energy harvesting from vibrations of the composite plates, but it can also be used to find damages like cracks and delamination. These damages cause a change in the natural frequency of the structure as well as

the output voltage of the piezoelectric patch, and by checking the voltage changes, it is possible to detect the type of damage and its location. Overall, the novelty of this work lies in its exploration of anisotropic effects in piezoelectric energy harvesting, providing valuable insights into the design and development of efficient piezoelectric structures for various applications in the aerospace, marine, and automotive industries. This novel approach sheds light on the potential for optimizing piezoelectric energy harvesting efficiency in plate-like structures, paving the way for advancements in energy harvesting technology.

Funding Statement

This research did not receive any specific grant from funding agencies in the public, commercial, or not-for-profit sectors.

Conflict of Interest

The authors declared no potential conflicts of interest with respect to the research, authorship, and publication of this article.

References

[1] Fatehi, P., Mahzoon, M., Farid, M., and Parandvar ,H., 2021. Modal reduction-based finite element method for nonlinear FG piezoelectric energy harvesters, Journal of Vibration and Control, 29, pp.362-374. https://doi.org/10.1177/10775463211048119.

[2] Ravi, S., Zilian, A., 2019. Simultaneous finite element analysis of circuit-integrated piezoelectric energy harvesting from fluid-structure interaction, Mechanical Systems and Signal Processing, 114, pp.259–274. https://doi.org/10.1016/j.ymssp.2018.05.016.

[3] Yaogang, W., Zhengguang, X., Dinghe, L., Jianxin, X., 2022. On numerical static analysis of stiffened laminated composite plates with delaminations, cracks, or debonding of a piezoelectric patch, Mechanics of Advanced Materials and Structures, 29, pp.89-103. https://doi.org/10.1080/15376494.2020.1751355.

[4] Muthalif, A. GA., Hafizh, M., Renno, J., Paurobally, M. R., 2021. An enhanced hybrid piezoelectric–electromagnetic energy harvester using dual-mass system for vortex-induced vibrations, Journal of Vibration and Control, 27, pp.2848-2861. https://doi.org/10.1177/10775463211041875.

[5] Fasihi, A., Shahgholi, M. and Ghahremani, S., 2021. The effects of nonlinear energy sink and piezoelectric energy harvester on aeroelastic instability of an airfoil, Journal of Vibration and Control, 28, pp. 1418-1432. https://doi.org/10.1177/1077546321993585.

[6] Ray, M. C., Jha, B. K., 2022. Exact solutions for bimorph cross-ply and antisymmetric angle-ply plate piezoelectric energy harvesters, Composite Structures, 286. https://doi.org/10.1016/j.compstruct.2022.115261.

[7] Song, J., Sun, G., Zeng, X. et al., 2022. Piezoelectric energy harvester with double cantilever beam undergoing coupled bending-torsion vibrations by width-splitting method, Scientific reports, 12, 583. https://doi.org/10.1038/s41598-021-04476-1.

[8] Krishnaswamy, J. A., Buroni, F. C., García-Macías, E., Melnik, R., Tembleque, L. R., Saez, A., 2020. Design of lead-free PVDF/CNT/BaTiO3 piezocomposites for sensing and energy harvesting: the role of polycrystallinity, nanoadditives, and anisotropy, Smart Materials and Structures, 29, 015021. https://doi.org/10.1088/1361-665X/ab547d.

[9] Topolov, V. Y., Isaeva, A. N., Bowen, C. R., Protsenko, B. O., 2021. Relationships between piezoelectric and energy-harvesting characteristics of 1–2–2 composites based on domain-engineered single crystals, Ferroelectrics, 583, pp.230-242.

[10] Bowen, C. R., Topolov, V. Y., Zhang, Y., Panich, A. A., 2018. 1-3-Type Composites Based on Ferroelectrics: Electromechanical Coupling, Figures of Merit, and Piezotechnical Energy-Harvesting Applications, Energy Technology, 6, pp.813-828.

[11] Topolov, V. Y., Isaeva, A. N., Bisegna, P., 2020. Novel lead-free composites with two porosity levels: large piezoelectric anisotropy and high sensitivity, Journal of Physics D: Applied Physics, 53, p. 395303.

[12] Raja, S., Sinha, P. K., Prathap, G., Bhattacharya, P., 2002. Influence of one and two dimensional piezoelectric actuation on active vibration control of smart panels, Aerospace Science and Technology, 6, pp. 209–216.

[13] Roscow, J. I., Topolov, V. Y., Taylor, J. T., Bowen, C. R., 2017. Piezoelectric anisotropy and energy-harvesting characteristics of novel sandwich layer BaTiO3 structures, Smart Materials and Structures, 26 105006. https://doi.org/10.1088/1361-665X/aa8348.

[14] Barrett, R., 1992. Active plate and wing research using EDAP elements, Smart Materials and Structures, 1: pp.214–226.
[15] Bent, A. A., Hagood, N. W., Rodgers, J. P., 1995. Anisotropic actuation with piezoelectric fibre composites, Journal of Intelligent Materials Systems and Structures, 6: pp.338–349.
[16] Rodgers, J. P., Hagood, N. W., 2012. Manufacture of Adaptive Composite Plates Incorporating Piezoelectric Fiber Composite Plies, AIAA-95-1096-CP, pp.2824–2835.
[17] Aridogan, U., Basdogan, I., Erturk, A., 2014. Analytical modeling and experimental validation of a structurally integrated piezoelectric energy harvester on a thin plate, Smart Materials and Structures, 23: 045039 (13pp). https://doi.org/10.1088/0964-1726/23/4/045039.
[18] Yoon, H., Youn, B. D., Kim, H. S., 2016. Kirchhoff plate theory-based electromechanically-coupled analytical model considering inertia and stiffness effects of a surface-bonded piezoelectric patch, Smart Materials and Structures, 25 025017 (18pp). https://doi.org/ 10.1088/0964-1726/25/2/025017.
[19] Paknejad, A., Rahimi, G., Salmani, H., 2018. Analytical solution and numerical validation of piezoelectric energy harvester patch for various thin multilayer composite plates, Archive of applied mechanics, 88, pp.1139-1161. https://doi.org/10.1007/s00419-018-1363-0.
[20] Chun, J., Kang, N., Kim, J., Noh, M., Kang, C., Choi, D., Kim, S., Wang, Z. L., Baik, J.M., 2015. Highly anisotropic power generation in piezoelectric hemispheres composed stretchable composite film for self-powered motion sensor, Nano Energy, 11, pp.1-10. https://doi.org/10.1016/j.nanoen.2014.10.010.
[21] Wakshume, D. G. and Płaczek, M. Ł. 2024. Optimizing Piezoelectric Energy Harvesting from Mechanical Vibration for Electrical Efficiency: A Comprehensive Review, Electronics, 13, (5), p. 987. https://doi.org/10.3390/electronics13050987.
[22] Tang, J., Wu, Y., Ma, S., Zhang, Y., Yan, T., Pan, Z., 2024.Three-directional knitted fabric sensor made of elastic carbon-based nanofiber yarn with excellent tensile and pressure sensing performance, Nano Energy, 128(A) 109801. https://doi.org/10.1016/j.nanoen.2024.109801.
[23] Bayik, B., Aghakhani, A., Basdogan, I., Erturk, A., 2016. Equivalent circuit modeling of a piezo-patch energy harvester on a thin plate with AC–DC conversion, Smart Materials and Structures, 25: 055015.
[24] Gharechae, A., Abazari, A., and Ketabdari, M.J., 2022. A semi-analytical solution for energy harvesting via the elastic motion of the circular floater of aquaculture cages attached with piezoelectric, Renewable Energy 196, pp.181-194.
[25] Stanton, S. C. et al., 2012. Nonlinear nonconservative behavior and modeling of piezoelectric energy harvesters including proof mass effects, Journal of Intelligent Materials Systems and Structures, 23, pp.183–99.
[26] Li, X., Upadrashta, D., Yu, K., Yang, Y., 2019. Analytical modeling and validation of multi-mode piezoelectric energy harvester, Mechanical Systems and Signal Processing, 124, pp.613–631. https://doi.org/10.1016/j.ymssp.2019.02.003.
[27] Tahmasbi, M., Jamshiddoust, A., Farrokhabadi, A., 2021. Optimum power of a nonlinear piezomagnetoelastic energy harvester with using multidisciplinary optimization algorithms, Journal of Intelligent Materials Systems and Structures, 32, pp.889-903. https://doi.org/10.1177/1045389X20974439.
[28] Qian, F., Liao, F., Zuo, L., Jones, P., 2021. System-level finite element analysis of piezoelectric energy harvesters with rectified interface circuits and experimental validation, Mechanical Systems and Signal Processing, 151, p. 107440. https://doi.org/10.1016/j.ymssp.2020.107440.
[29] Erturk, A., Inman, D. J., 2011. Piezoelectric Energy Harvesting. Wiley, Hoboken.
[30] Marqui Junior, C. D., Erturk, A., Inman, D. J., 2009. An electromechanical finite element model for piezoelectric energy harvester plates, Journal of Sound and Vibration, 327, pp. 9-25. doi.org/10.1016/j.jsv.2009.05.015.
[31] Leissa, W., 1969. Vibration of plates, NASA SP-160.
[32] Meirovitch, L., 2001. Fundamentals of Vibration International, McGraw-Hill Higher Education.
[33] Farrokhabadi, A., Neyestani, S., Akbari, D., Sarkhosh, R., 2021. Assessment of delamination growth due to matrix cracking in hybrid Glass-Kevlar composite laminates using experimental, numerical and analytical methods, Engineering Fracture Mechanics, 247, p. 107691.